Ricin A-Chain Inhibitors Resembling the Oxacarbenium Ion Transition State†

Kelly S. E. Tanaka,‡ Xiang-Yang Chen,§ Yoshitaka Ichikawa,|| Peter C. Tyler,⊥ Richard H. Furneaux,⊥ and Vern L. Schramm*,‡

Department of Biochemistry, Albert Einstein College of Medicine, 1300 Morris Park Avenue, Bronx, New York 10461, Pharmacia Corporation, Mail Zone Q3A, 800 North Lindbergh Boulevard, St. Louis, Missouri 63167, Department of Pharmacology and Molecular Sciences, Johns Hopkins School of Medicine, Baltimore, Maryland 21205, and Carbohydrate Chemistry Team, Industrial Research Ltd., Lower Hutt, New Zealand

Received March 12, 2001; Revised Manuscript Received April 19, 2001

ABSTRACT: Ricin toxin A-chain (RTA) is expressed by the castor bean plant and is among the most potent mammalian toxins. Upon activation in the cytosol, RTA depurinates a single adenine from position 4324 of rat 28S ribosomal RNA, causing inactivation of ribosomes by preventing the binding of elongation factors. Kinetic isotope effect studies have established that RTA operates via a $D_N{*}A_N$ mechanism involving an oxacarbenium ion intermediate with bound adenine [Chen, X.-Y., Berti, P. J., and Schramm, V. L. (2000) *J. Am. Chem. Soc. 122*, 1609−1617]. On the basis of this information, stem−loop RNA molecules were chemically synthesized, incorporating structural features of the oxacarbenium ion-like transition state. A 10-base RNA stem−loop incorporating (1*S*)-1-(9-deazaadenin-9-yl)-1,4-dideoxy-1,4-imino-D-ribitol at the depurination site binds four times better (0.57 μM) than the 10-base RNA stem−loop with adenosine at the depurination site (2.2 μM). A 10-base RNA stem−loop with 1,2-dideoxyribitol [(2*R*,3*S*)-2-(hydroxymethyl)-3-hydroxytetrahydrofuran] at the depurination site binds with a K_d of 3.2 μM and tightens to 0.75 μM in the presence of 9-deazaadenine. A similar RNA stem−loop with 1,4-dideoxy-1,4-imino-D-ribitol at the depurination site binds with a K_d of 1.3 μM and improves to 0.65 μM with 9-deazaadenine added. When (3*S*,4*R*)-4-hydroxy-3-(hydroxymethyl)pyrrolidine was incorporated at the depurination site of a 14-base RNA stem−loop, the K_d was 0.48 μM. Addition of 9-deazaadenine tightens the binding to 0.10 μM whereas added adenine increases the affinity to 12 nM. The results of this study are consistent with the unusual dissociative $D_N{*}A_N$ mechanism determined for RTA. Knowledge of this intermediate has led to the design and synthesis of the highest affinity inhibitor reported for the catalytic site of RTA.

Ricin is a cytotoxic heterodimeric protein found in the seeds of the castor bean plant *Ricinus communis* (*1*). Ricin toxin A-chain (RTA)[1] is a highly specific *N*-glycosidase (Figure 1). It catalyzes the hydrolysis of a single adenosine residue, A^{4324} of rat 28S ribosomal RNA, at a facile rate of 1777 min^{-1} (*2*, *3*). The base-exposed secondary structure of A^{4324} results from its location at the second position of a GNRA tetraloop in stem−loop RNA (*4*). RTA is catalytically active on only the first adenine of the GAGA sequence and only in the framework of a stem−loop structure (*5*, *6*). Short RNA structures possessing a stem of at least three base pairs and a GAGA stem−loop are also substrates for RTA (*5*, *7*, *8*). At physiological pH, short RNA stem−loops have k_{cat} values of approximately 10^{-5} that for intact ribosomes (*5*, *7*, *9*, *10*). At pH values near 4, however, short RNA GAGA stem−loops are active substrates. Specifically, at pH 4.1 the 10- and 14-mers, **A-10** and **A-14** (Figure 2a) have k_{cat} values of 4.1 and 219 min^{-1}, respectively (*11*). The K_m values for both substrates are similar, and the rate for **A-14** is within an order of magnitude of that for RTA on intact ribosomes (*3*).

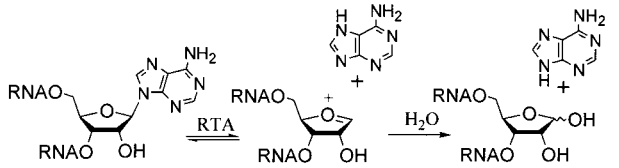

FIGURE 1: Hydrolytic reaction catalyzed by ricin A-chain. The oxacarbenium ion intermediate is shown. The lifetime of the illustrated oxacarbenium ion intermediate is not known but is estimated to be between approximately 10^{-12} s and the k_{cat} for RTA (*15*). At the TS and enzyme-bound intermediate, protonation of adenine at N7 will be preferred.

Combining the RTA toxin with antibodies specific for cancer cell epitopes results in an immunotoxin that has considerable activity as an anticancer drug (*12*, *13*). Unfortunately, vascular leak syndrome is a limiting and severe side effect in clinical trials (*13*). Inhibitors for RTA may be

† This work was supported by National Institutes of Health Research Grants GM52324 (to Y.I.) and CA72444 (to V.L.S.).

* Corresponding author. Tel: (718) 430-2813. Fax: (718) 430-8565. E-mail: vern@aecom.yu.edu.

‡ Albert Einstein College of Medicine.

§ Pharmacia Corp.

|| Johns Hopkins School of Medicine.

⊥ Industrial Research Ltd.

[1] Abbreviations: 4-APP, 4-aminopyrazolo[3,4-*d*]pyrimidine; 8-AA, 8-azaadenine; 9-DA, 9-deazaadenine; CPG, controlled pore glass; DMF, *N*,*N*-dimethylformamide; DMAP, 4-(dimethylamino)pyridine; DMTr, dimethoxytrityl; Fmoc, 9-fluorenylmethoxycarbonyl; KIE, kinetic isotope effect; MALDI, matrix-assisted laser desorption ionization; RTA, ricin toxin A-chain; TBDMS, *tert*-butyldimethylsilyl; TS, transition state.

10.1021/bi010499p CCC: $20.00
Published on Web 05/16/2001

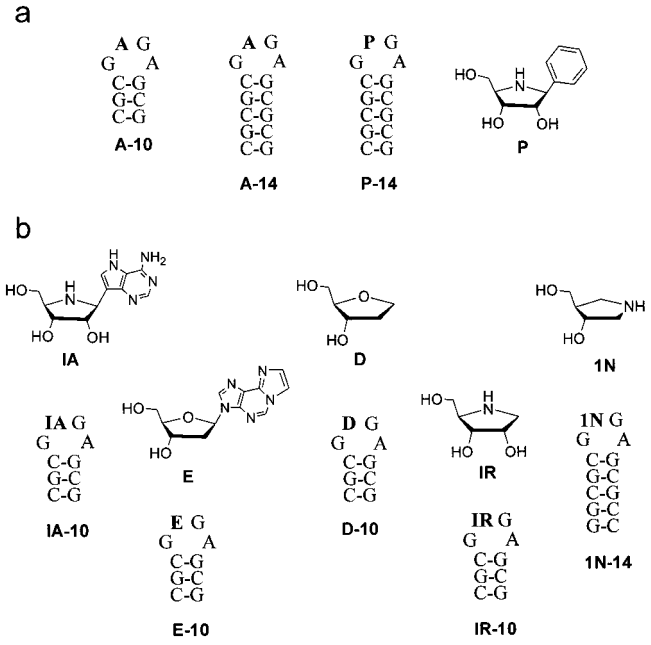

FIGURE 2: Short RNA stem−loop substrates (**A-10** and **A-14**) and inhibitor (**P-14**) for RTA (a). The five short RNA stem−loop-based inhibitors of the present study (b).

useful antidotes against this class of potent toxins and may serve to ameliorate vascular leak syndrome, a side effect which is believed to be a result of the nonspecific toxicity against the capillary vasculature (*13*, *14*). Furthermore, potent inhibitors of RTA may also prove useful for a more detailed understanding of the catalytic mechanism of RTA, including the testing of the recent transition state (TS) proposals for this enzyme (*15*, *16*). In the initial inhibitor design, it was assumed that RTA stabilizes a TS similar to other purine nucleoside *N*-glycosidases, where the TS has been determined to be oxacarbenium[2] ion-like with low residual bond order to the leaving group (*17*). For example, incorporating the known nucleoside *N*-ribohydrolase inhibitor, phenyliminoribitol (*18*), at the depurination site of the RNA stem−loop 14-mer (**P-14**, Figure 2a) resulted in an RTA inhibitor with a K_i of 0.18 μM (*11*, *19*).

Recently, kinetic isotope effects (KIEs) analyzed by bond vibrational and quantum chemical approaches were completed for the RTA-catalyzed hydrolysis of **A-10** (*15*). These results established an unprecedented mechanism for *N*-glycosidases, one that follows the highly dissociative stepwise $D_N{*}A_N$ mechanism with oxacarbenium ion-like TSs (*15*, *16*). A dissociative mechanism has subsequently been implicated for the pyrimidine-specific uracil DNA glycosidase (*20*). In the present study, several short RNA stem−loop compounds were synthesized to further investigate the dissociative nature of the RTA reaction (Figure 2b). These compounds were designed to explore the prediction of the TS structure. Specifically, the transition state analysis predicts that abasic (lacking the adenine ring) RNA stem−loops with oxacarbenium ion mimics should bind more tightly than RNA stem−loops with covalent *C*-nucleoside mimics of oxacarbenium ions. Furthermore, this TS analysis predicts that adenine or adenine analogues should enhance binding of the abasic RNA stem−loop oxacarbenium ion mimics since this combination most closely resembles the tightly bound intermediates defined by the $D_N{*}A_N$ mechanism.

[2] The International Union of Pure and Applied Chemistry designates replacement of a carbon by an oxygen atom to be termed "oxa" whereas the nomenclature for a carbon atom replaced by a carbonyl group is "oxo".

EXPERIMENTAL PROCEDURES

General Experimental. RTA was purchased from Inland Laboratories (Austin, TX). Calf intestinal alkaline phosphatase was purchased from Promega (Madison, WI), and phosphodiesterase I was from Sigma Chemical Co. (St. Louis, MO). RNase inhibitors and RNase-free DNase were received from Ambion (Austin, TX). Nucleoside phosphoramidites and other reagents for oligoribonucleotide synthesis were purchased from Glen Research (Sterling, VA) except for phosphoramidites attached directly to CPG solid supports, which were obtained from ChemGene Corp. (Ashland, MA). [2,8-^{3}H]Adenosine triphosphate (42 Ci/mmol) was purchased from Amersham Pharmacia (Piscataway, NY). 8-Azaadenine was purchased from Fluka Chemical Corp. (Milwaukee, WI). The adenine analogue 9-deazaadenine was a product of Industrial Research Ltd., Lower Hutt, New Zealand. All other chemicals were purchased from Aldrich Chemical Co. (Milwaukee, WI) and were of the highest purity available. These reagents were used without further purification.

Purification of reaction intermediates of the phosphoramidite synthetic pathway was completed by flash column chromatography using Merck silica gel 60 (230−400 mesh). Purification by HPLC was performed on a Waters 626 pump with a 996 photodiode array detector and using the Millennium^{32} software package. RNA concentrations were determined by UV/vis measurements using a HP 8453 diode array spectrophotometer. Radioactivity measurements were completed on a Wallac 1414 scintillation counter using liquiscint scintillation fluid.

Synthesis of the Radiolabeled Substrate (**[^{3}H]A-10**). Stem−loop RNA 10-mer labeled with [2,8-^{3}H]adenine (**[^{3}H]A-10**) was synthesized as described previously (*15*) using commercially available T7 RNA polymerase (Ambion, Austin, TX). The primer and template sequences were the same as those used by Chen et al. (*15*). Reaction mixtures contained 5.0 mM GTP, 3.0 mM CTP, 0.50 mM ATP, 10^7 cpm of [2,8-^{3}H]ATP, 0.5 μM DNA template-primer, RNase inhibitor (40 units), and T7 RNA polymerase (3000 units). After incubation for 10−12 h at 37 °C, RNase-free DNase (10 units) was added, and the reaction mixture was incubated for an additional 30 min at 37 °C. The RNA was precipitated by the addition of 99% ethanol (3.5 equiv, v/v) and cooling to −70 °C after Na_2EDTA and NaOAc were added to a final concentration of 50 and 400 mM, respectively. Purification of **[^{3}H]A-10** was completed by denaturing (7 M urea) 24% PAGE electrophoresis. RNA product bands were located by UV shadowing and were extracted into 1.0 M NaOAc (5 mL) (*21*). Incorporation of radioactivity was determined by liquid scintillation counting.

Synthesis of the Nucleoside Phosphoramidite Analogues. Synthesis of the 1,4-dideoxy-4-imino-D-ribitol phosphoramidite (**5**) was completed as illustrated in Scheme 1. The amine (**1**) in methanol was treated with 9-fluorenylmethyl chloroformate and triethylamine to afford, after column chromatography (CH_2Cl_2/MeOH/H_2O, 50:1:0.1 v/v/v), the *N*-fluorenylmethoxycarbonyl- (Fmoc-) protected compound

Scheme 1[a]

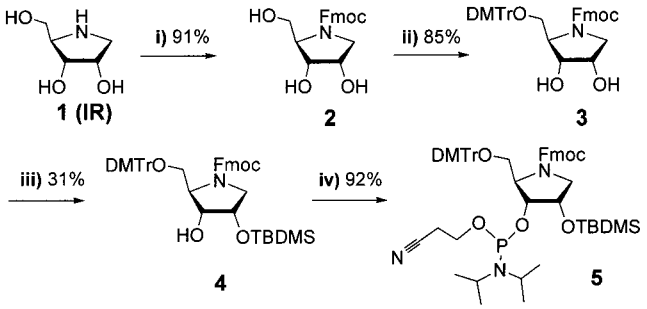

[a] Conditions: (i) FmocCl (2 equiv), Et_3N (4 equiv), MeOH, room temperature, 4 h; (ii) DMTrCl (1.5 equiv), DMAP(cat), $(iPr)_2NEt$ (2 equiv), pyridine, room temperature, 6 h; (iii) TBDMSCl (1.5 equiv), imidazole (5 equiv), DMF, room temperature, 12 h; (iv) 2-cyanoethyldiisopropyl chlorophosphoramidite (2 equiv), $(iPr)_2NEt$ (4 equiv), CH_2Cl_2, room temperature, 3 h.

Scheme 2[a]

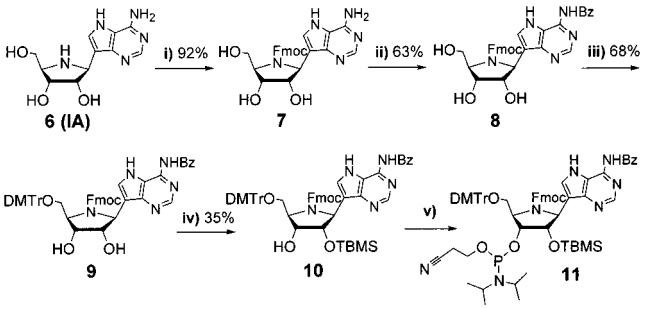

[a] Conditions: (i) FmocCl (1.8 equiv), pyridine (2 equiv), MeOH, room temperature, 4 h; (ii) (a) TMSCl (12 equiv), pyridine, room temperature, 1 h, then BzCl (1.4 equiv), room temperature, 3 h, and then quench with H_2O, (b) acetic acid in MeOH (10% v/v), room temperature, 3 h, (c) trimethylamine in methanol (10% v/v), room temperature, 1 h; (iii) DMTrCl (1.5 equiv), DMAP(cat), $(iPr)_2NEt$ (5 equiv), CH_2Cl_2, room temperature, 4 h; (iv) TBDMSCl (3.6 equiv), imidazole (5 equiv), DMF, room temperature, 4 h; (v) 2-cyanoethyldiisopropyl chlorophosphoramidite (2.5 equiv), 2,4,6-collidine (7.5 equiv), *N*-methylimidazole (0.5 equiv), CH_2Cl_2, room temperature, 3 h.

(**2**). The 5-OH was converted to the dimethoxytrityl (DMTr) ether **3** by reacting **2** with DMTrCl in anhydrous pyridine using DMAP as the catalyst, followed by standard workup and purification by column chromatography (CH_2Cl_2/MeOH/H_2O, 35:1:0.1 v/v/v). Silylation of **3** with *tert*-butyldimethylsilyl chloride (TBDMSCl) resulted in a mixture of isomers that were separated by column chromatography (CH_2Cl_2/MeOH/H_2O, 20:1:0.1 v/v/v). The 2-*O*-TBDMS-protected compound **4** was reacted with 2-cyanoethyl diisopropylchlorophosphoramidite in the presence of diisopropylethylamine to give the phosphoramidite **5** that was purified by column chromatography (ethyl acetate/toluene, 1:15 v/v). Compound **5** was used toward the synthesis of **IR-10**.

The phosphoramidite of (1*S*)-1-(9-deazaadenin-9-yl)-1,4-dideoxy-1,4-imino-D-ribitol, **IA** (*22*), was synthesized from the precursor **6** in five steps (Scheme 2). The iminoribitol derivative (**6**) in methanol was treated with 9-fluorenylmethyl chloroformate and pyridine to give the *N*-Fmoc-protected compound **7** after column chromatography. A solution of **7** in pyridine was cooled in an ice bath followed by the addition of trimethylsilyl chloride. The resulting solution was stirred at room temperature for 1 h, and then benzoyl chloride (0.27 mL) was added after cooling to 0 °C. The resulting solution was stirred at room temperature for 3 h before being poured into water. The mixture was extracted twice with chloroform, and the combined extracts were dried and concentrated to dryness. The residue was dissolved in methanol containing 10% acetic acid (v/v), and the solution was allowed to stand for 3 h and then concentrated to dryness. The residue was dissolved in methanol and triethylamine (10%, v/v), and after 1 h the solution was concentrated to dryness and purified by column chromatography to afford compound **8**. A solution of **8** in dichloromethane was treated with diisopropylethylmine, DMAP, and DMTrCl. After the standard workup procedure the residue was purified by column chromatography to give **9**. A solution of **9** in DMF containing imidazole was treated with TBDMSCl to afford compound **10** after column chromatography (ethyl acetate/hexanes, 1:3 v/v). Compound **10** was reacted with 2-cyanoethyl diisopropylchlorophosphoramidite in the presence of 2,4,6-collidine and *N*-methylimidazole to give **11**, which was used without purification in the synthesis of **IA-10**. The 1-aza-1,2-dideoxy-4a-carba-D-ribitol, **1N** (*23*), phosphoramidite used in the synthesis of **1N-14** was prepared as described previously (*23*, *24*).

Synthesis and Purification of Oligoribonucleotides. Oligonucleotides were chemically synthesized using phosphoramidite methodology on an Applied Biosystems 391 DNA synthesizer at the 1 μmol scale with coupling times extended to 15 min, in the trityl-off mode. Deprotection of the products was accomplished using concentrated NH_4OH/ethanol (3:1 v/v) (*25*, *26*) and triethylamine trihydrofluoride (*27*) as described by Chen et al. (*11*). All products were purified by HPLC using Nucleogen DEAE 60-7 (125 × 4) ion-exchange chromatography followed by ion-pairing reverse-phase C18 μBondpak column chromatography. The ion-exchange chromatography buffer system was 50 mM ammonium acetate (pH 5.0) in 15% methanol, eluting with a linear gradient of 50 mM ammonium acetate (pH 5.0) containing 1.0 M LiCl. For reverse-phase chromatography the buffer system was 50 mM triethylammonium acetate (pH 7.8), eluting with a linear gradient of methanol. Compound identity was verified by enzymatic digestion to nucleosides using alkaline phosphatase and phosphodiesterase I followed by HPLC analysis (*11*). Product formation for all RNA stem−loop compounds was further confirmed by MALDI-TOF mass spectrometry analysis, performed by Dr. Haiteng Deng at the Laboratory for Macromolecular Analysis and Proteomics at the Albert Einstein College of Medicine.

Inhibition Kinetics. Reaction rates were determined in 10 mM sodium citrate buffer (pH 4.0) containing 1 mM EDTA using **[^{3}H]A-10** with carrier **A-10** as the substrate. Concentrations of **A-10** were maintained near the K_m value, using approximately 1.0×10^4 cpm in a total volume of 50 μL. Inhibitor (stem−loop or purine) concentrations were varied while keeping the **A-10** at a constant concentration. After incubation of the reaction vials at 37 °C for the allotted time (less than 15% conversion) the reactions were quenched by the addition of 100 mM potassium phosphate buffer (pH 8.3, 25 μL). The [2,8-^{3}H]adenine product was isolated by passing the reaction mixture through a small column of DEAE-cellulose (Whatman DE52, approximately 0.75 mL in a Pasteur pipet) and analyzed by scintillation counting. Values for the inhibition dissociation constant (K_i) were determined using the equation for competitive inhibition: $v = k_{cat}$

$S/(S + K_m(1 + I/K_i))$, where v is the initial reaction rate, S is the substrate concentration, K_m is the Michaelis constant, I is the inhibitor concentration, and k_{cat} is the catalytic turnover number. For rates involving a ternary complex the substrate and stem−loop inhibitor concentrations were kept constant and the purine concentration was varied. The K_i values for these compounds were determined using the thermodynamic cycle shown in Figure 5.

Exchange Reaction. Exchange reactions were carried out at 37 °C in 10 mM sodium citrate buffer (pH 4.0), 1.0 mM EDTA, 40 nM RTA, 10.2 μM unlabeled **A-10,** and 1.0 or 1.5 mM adenine with approximately 7.0×10^5 cpm of [2,8-^{3}H]adenine per reaction. The reactions were initiated by the addition of either RTA or **A-10**, allowing for incubation of substrate with adenine or RTA and adenine, respectively. The reactions were allowed to continue to approximately 10% completion and then quenched by the addition of 100 mM potassium phosphate buffer (pH 8.3, 25 μL). Adenine was separated from the substrate by passing the reaction mixture through a DEAE-cellulose (Whatman DE52) column. The substrate was then eluted with 50 mM ammonium acetate (pH 5.5) containing 1 M LiCl and analyzed for radioactivity by scintillation counting.

RTA Assay Using Fluorescence Spectroscopy. The RTA assay was monitored using a Spectromax-3 fluorescence spectrophotometer set at 5 mm slit widths using **E-10** as the potential substrate. The change in fluorescence was monitored at an emission wavelength of 405 nm and an excitation wavelength of 275 nm. The reactions were carried out at 37 °C in 10 mM sodium citrate buffer (pH 4.0) containing 1.0 mM EDTA with 400 nM RTA and 8.0 μM **E-10**. The emission spectra (350−500 nm) were also monitored over a 30 min period using 4.0 μM **E-10** and 100 nM RTA.

RESULTS AND DISCUSSION

Inhibition of RTA with RNA Stem−Loop Analogues. The fluorescent adenine derivative, etheno-2′-deoxyadenine, was incorporated into a 10-mer RNA stem−loop resulting in compound **E-10** (Figure 2b). This compound was first evaluated as a substrate for RTA using fluorescence spectroscopy. No change in the fluorescence intensity at 405 nM was detected when **E-10** (8 μM) was incubated with RTA (400 nM) at 37 °C. Under the assay conditions the fluorescence intensity of ethenoadenine is 1.5 times that of ethenoadenosine; thus 5% conversion of **E-10** to products would be readily detected. The lack of substrate activity for **E-10** is consistent with the RTA reaction mechanism, which relies on specific leaving group interactions without nucleophilic assistance toward the formation of the oxacarbenium ion intermediate. Although binding constants were not reported, it is has been demonstrated that an RNA stem−loop 12-mer with deoxyadenosine at the depurination site is hydrolyzed approximately 26 times faster than the corresponding RNA stem−loop 12-mer (*9*). Thus, the 2-deoxyribitol moiety is not responsible for the inability of RTA to utilize **E-10** as a substrate. Furthermore, nonspecific inosine−uridine *N*-ribohydrolases, which operate through oxacarbenium ion TSs (*17*), are known to accept ribosyl compounds with good leaving groups as substrates whereas the substituent-specific enzymes do not (*28*, *29*). Consistent with this evaluation, RTA does not hydrolyze either 4-nitrophenyl β-D-ribofuranoside (*11*) or etheno-2′-deoxyadenosine in the context of stem−loop RNA substrates.

Table 1: Kinetic Constants for RTA-Catalyzed Reaction with the Substrates **A-10** and **A-14** and Competitive Inhibition Constants for the Inhibitors **P-14**, **IA-10**, and **E-10**

substrate	K_m (μM)[a]	inhibitor	K_i (μM)[b]
A-10	2.2 ± 0.5	**P-14**	0.18 ± 0.02[c]
A-14	8.1 ± 0.7[c]	**IA-10**	0.57 ± 0.06
		E-10	4.2 ± 0.6

[a] Kinetic constants were obtained from fits of the initial rate data versus substrate concentrations to the Michaelis−Menten equation.[b] K_i values were determined from fits of initial rate data versus inhibitor concentration to the equation $v = k_{cat}S/(S + K_m(1 + I/K_i))$. [c] Value taken from ref *11*.

E-10 was evaluated as an inhibitor, and a K_i value of 4.2 ± 0.6 μM was determined, approximately double the K_m value of 2.2 ± 0.5 μM obtained for **A-10** (Table 1). RTA exhibits fully expressed KIEs, establishing equilibrium with the RNA stem−loop prior to a chemical step (*15*). The K_m values for **A-10** are therefore equivalent to dissociation constants, as are K_i values for competitive inhibitors. Thus the extra bridge of the etheno substituent has a small steric effect toward binding, altering affinity by only 2-fold. Although absence of the 2′-hydroxyl increases the rate of hydrolysis for a substrate, its effect toward binding is unknown (*9*).

IA-10 has the nonhydrolyzable 9-deazaadenine iminosugar immucillinA (**IA**)[3] incorporated into a 10-mer RNA stem−loop (Figure 2b). The endocyclic nitrogen atom of this compound mimics the oxacarbenium ion nature of the ribosyl ring at the transition state of the RTA-catalyzed hydrolysis of **A-10** (*15*). In addition, the pK_a of N7 in 9-deazaadenosine is above 12 (*30*). These features ensure that the 9-deazaadenyl ring resembles an acid-activated leaving group while the iminoribitol ring mimics the oxacarbenium ion. In addition, **IA** is a powerful TS analogue inhibitor of purine nucleoside *N*-ribosylhydrolases that accept adenosine as a substrate (*31*). Since the 9-deazaadenyl substituent more closely resembles the adenyl substituent at the TS, it is somewhat surprising that **P-14** (*11*, *19*) binds approximately 2.5 times better than **IA-10** and that **IA-10** binds only four times better than **A-10** (Figure 4a, Table 1). These results, however, are consistent with the KIE study that describes the RTA mechanism as being highly dissociative (*15*). In this mechanism considerable separation between the ribosyl moiety and the leaving group adenine has occurred at the first TS. Thus, the 9-deazaadenyl substituent in **IA-10** is constrained in its ability to mimic the dissociation of the adenyl substituent at the actual TS due to the covalent C−C ribosidic bond. This constraint causes unfavorable interactions between the 9-deazaadenyl substituent and the RTA active site. At the TS, the enzyme has activated the leaving group and distanced it from the ribosyl ring prior to nucleophilic attack by water. By comparison, the simple hydrophobic interaction of the smaller phenyl group in **P-14** binds three times better than **IA-10**, even though it cannot access the adenine leaving group interactions required for TS formation (Table 1).

RTA Inhibition by Abasic RNA Stem−Loop Analogues. **D-10**, **IR-10**, and **1N-14** possess abasic residues at the

[3] ImmucillinA, (1*S*)-1-(9-deazaadenin-9-yl)-1,4-dideoxy-1,4-imino-D-ribitol.

Table 2: Inhibition Kinetic Constants for the Three Abasic RNA Stem−Loop Inhibitors of the RTA-Catalyzed Reaction with the **A-10** Substrate

	K_i (μM)[a]			
	without	stem−loop inhibitor		
purine	stem−loop	**1N-14**	**IR-10**	**D-10**
		0.48 ± 0.08	1.3 ± 0.2	3.2 ± 0.9
adenine	1000[b]	0.012	*c*	*c*
9-DA[d]	340 ± 50	0.10	0.65	0.75
8-AA[e]	60[b]	*f*	*f*	*f*
4-APP[g]	300[b]	*c*	*c*	*c*

[a] K_i values were determined from fits of initial rate data versus inhibitor concentration to the equation $v = k_{cat}S/(S + K_m(1 + I/K_i))$. [b] Estimated K_d values for activation reaction rates. [c] No effect. [d] 9-Deazaadenine. [e] 8-Azaadenine. [f] Activation in the reaction rate was observed but not quantified. [g] 4-Aminopyrazolo[3,4-*d*]pyrimidine.

reaction site that are useful in determining the relative contribution of the adenyl substituent and the oxacarbenium ion toward binding (Figure 2b). These compounds also indicate the atomic geometry for the enzyme-stabilized positive charge that develops within the ribosyl ring at the TS. The K_i values for **D-10**, **IR-10**, and **1N-14** are 3.2, 1.3, and 0.48 μM, respectively (Table 2). As expected for an oxacarbenium ion TS, the neutral **D-10** was the weakest of the three abasic RNA stem−loop inhibitors. However, **D-10** and **A-10** bind with almost equal affinity, a surprising result based on the presumed binding energy available from the adenine ring. Dissociation constants are the sum of binding and distortional energies; thus it is feasible that substantial ground state destabilization occurs with **A-10** but is missing with **D-10**. The neutral **D-10** binds approximately 2.5 and 6.5 times less tightly than **IR-10** and **1N-14**, respectively. Although these constants demonstrate increased affinity with positive charge in the iminoribitol ring, they are relatively small increases compared to those expected for full TS interaction. The pK_a values of the endocyclic nitrogen at both the 1- and 4-positions are approximately 6.5, ensuring that they will be positively charged under the assay conditions (pH 4). The 2.5 times more favorable binding of the "1-azasugar" **1N-14** relative to the "iminosugar" **IR-10** (Table 1, Figure 4e and Figure 4b, respectively) indicates differences in the electronic nature of the rate-limiting TS for RTA compared with other *N*-glycosidases. A similar trend was found for inhibitors for 3-methyladenosine DNA glycosidase II where DNA 25-mers, which incorporated **IR** and **1N**, were determined to have dissociation constants of 16 pM and approximately 0.1 nM, respectively (*24*, *32*). With regard to hexopyranosides, the 1-azasugars are known to be better inhibitors than the corresponding iminosugars for a number of β-glycosidase enzymes (*33*−*38*). Recently, it has been determined that differences in β-glucosidase inhibitor potency between 1-deoxynojirimycin and isofagomine, the paradigmatic iminosugar and 1-azasugar, respectively, arise largely from the large positive entropy for the latter upon binding (*39*). Although the ribofuranoside substrates for *N*-glycosidases are always the β-anomers, the increased efficacy of **1N-14** may be typical for enzymes that operate via a $D_N{*}A_N$ mechanism, such as RTA or DNA glycosidase II.

RTA Activation and Inhibition by Adenine Analogues. The dissociated intermediate near the TS of RTA-catalyzed hydrolysis predicts that inhibitors should contain oxacarbenium ion character in the ribosyl ring and include a

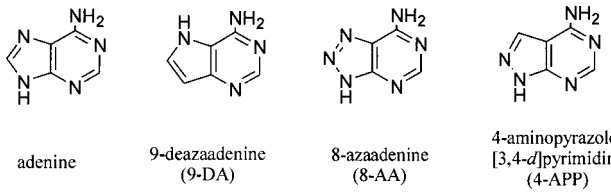

FIGURE 3: Adenine and the adenine analogues 4-aminopyrazolo-[3,4-*d*]pyrimidine (4-AA), 8-azaadenine (8-AA), and 9-deazaadenine (9-DA) used in this study.

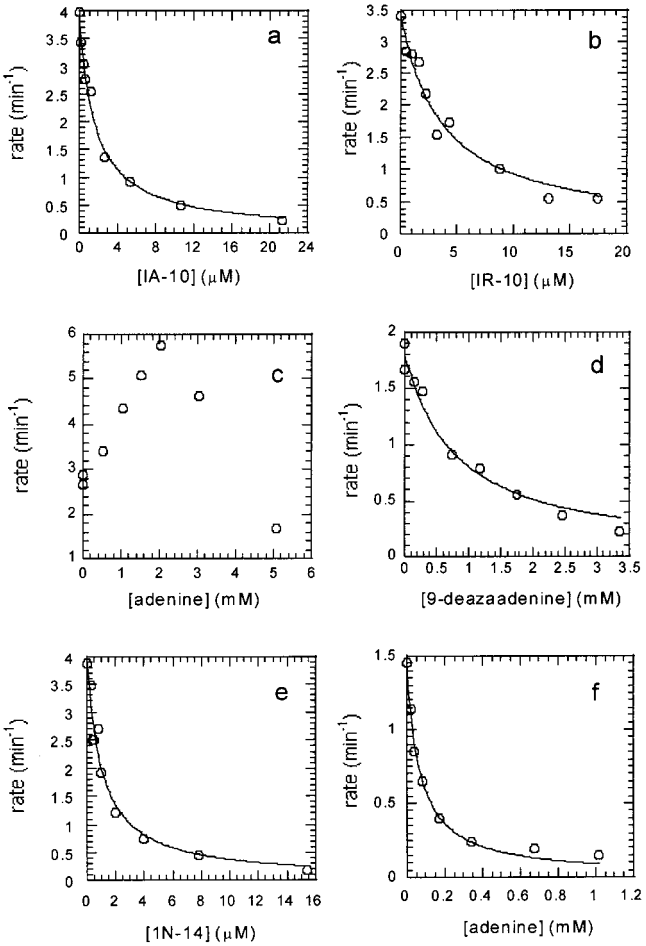

FIGURE 4: Plots for the RTA-catalyzed hydrolysis of **A-10** at pH 4.0 with the addition of the RNA stem−loop inhibitor, purine, or both. Inhibition by RNA stem−loop compound **IA-10** (a) or abasic RNA stem−loop compound **IR-10** (b). Activation by adenine (c). Inhibition by the adenine analogue 9-deazaadenine (d). Inhibition by the abasic RNA stem−loop compound **1N-14** (e). Inhibition with constant **1N-14** (1.6 μM) and added adenine (f).

dissociated adenine ring. Combinations of abasic stem−loop RNA analogues with adenine analogues were tested for this reason. The effects of four different adenine analogues (Figure 3) were evaluated in the absence and presence of the abasic RNA stem−loop inhibitors. As a control for these experiments, the effects of adenine-based analogues and stem−loop elements were tested alone and together as inhibitors with respect to substrate. Adenine (Figure 4c), 8-azaadenine (8-AA), and 4-aminopyrazolo[3,4-*d*]pyrimidine (4-APP) were all found to increase the rate of RTA-catalyzed **A-10** hydrolysis in the absence of abasic RNA stem−loop inhibitors followed by inhibition at higher concentrations. The estimated dissociation constants are listed in Table 2. The dissociation constant of 1 mM for adenine has also been determined using fluorescence spectroscopy (*40*). An un-

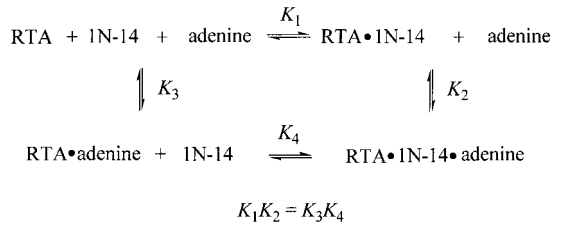

FIGURE 5: Thermodynamic cycle for the binding of the ternary complex of **1N-14**, adenine, and RTA. K_i for the ternary complex was determined by solving for K_4 using the K_1 value determined from the data illustrated in Figure 4e (0.48 μM), K_2 was determined from the data shown in Figure 4f (24 μM), and K_3 was estimated from the data in Figure 4c (1000 μM), the same dissociation value as that determined by fluorescence spectroscopy (*40*).

competitive inhibition constant value for adenine was found to be approximately 30 μM, but these authors used an indirect ricin assay with intact ribosomes as the substrate at pH 7.4 (*41*). Surprisingly, 9-deazaadenine (9-DA) was the only compound found to give the expected product inhibition pattern (K_i = 340 μM) rather than the combination of activation followed by inhibition (Figure 4d). One possible explanation for the observed activations is that these purines are enhancing an adenine exchange reaction in which added purine is exchanged into the labeled **A-10** stem−loop substrate, thus increasing the extent of labeled adenine release. This would be consistent with the result that nonexchangeable 9-deazaadenine did not increase the rate of [2,8-^{3}H]adenine release. Unlabeled **A-10** was incubated with RTA in the presence of an excess amount of labeled adenine to determine if the radioisotope would be incorporated into the substrate during the first 10% of **A-10** hydrolysis. The reaction conditions would have permitted the detection of a 1% exchange of adenine (0.1 μM) into unreacted **A-10**. No radioactivity was found in the recovered **A-10** substrate, consistent with similar experiments reported earlier for RTA (*15*). Thus adenine analogues increase the catalytic turnover rate by binding at a remote site or by increasing the rate of an enzyme isomerization after the irreversible chemical step.

Enhanced Inhibition by Analogues of the Transition State. The most striking inhibition data were found for the effects of added adenine in the presence of the abasic RNA stem−loop inhibitor **1N-14** (Figure 4e). Although adenine is an activator of the reaction up to concentrations of approximately 2 mM, in the presence of 0.96 or 1.6 μM **1N-14**, a K_i of 24 μM was found for adenine (Figure 4f). Using the thermodynamic equilibrium for substrate and inhibitors (Figure 5) the K_i value for the ternary complex was calculated to be 12 nM. Thus, the combination of stem−loop oxacarbenium ion mimic together with adenine binds approximately 180 times tighter than **A-10** substrate. It is remarkable that neither **IR-10** nor **D-10** had similar inhibition kinetics with added adenine whereas all three abasic RNA stem−loop inhibitors demonstrated similar but smaller binding enhancements with 9-deazaadenine.

Although there is no structural data for a stem−loop RNA−RTA complex, there are X-ray crystallographic data for adenine, adenyl(3′−5′)guanosine, formycin monophosphate, pterin, and neopterin complexes with RTA (*42*−*44*). The structures with adenine analogues have interactions between the purine ring and the residues Tyr80, Tyr123, and Ile172. There are also contacts between the ribose ring and Glu177 and Glu203 for the formycin monophosphate and adenyl(3′−5′)guanosine complexes. From these crystallographic data it is apparent that the adenyl moiety has increased contacts with the active site residues compared to depurinated stem−loop RNA. This would explain the enhanced inhibition of **1N-14** in the presence of adenine. The inhibition data presented here indicate that, aside from favorable protein−stem−loop interactions, the abasic nitrogen atom of **1N-14** forms a hydrogen bond with N9 of the adenine ring that helps to orient and anchor the stem−loop RNA within the active site.

The specific enhanced binding by **1N-14** and adenine relative to **IA-10** or **A-10** can be attributed to the reconstitution of the components most similar to the transition state, even though these have been separated into distinct pieces. Wolfenden and colleagues have investigated the effect of TS inhibitors in pieces and found a loss of 7−10 kcal/mol binding energy from loss of covalent integrity (*45*, *46*). When these factors are applied to the present case, the results suggest that inhibitors would bind in the 1.4−170 pM range if the appropriate linker can be found to connect adenine analogues to the oxacarbenium ion analogues in stem−loop RNA.

REFERENCES

1. Olsnes, S., and Pihl, A. (1973) *Biochemistry 12*, 3121−3126.
2. Endo, Y., and Tsurugi, K. (1987) *J. Biol. Chem. 262*, 8128−8130.
3. Endo, Y., and Tsurugi, K. (1988) *J. Biol. Chem. 263*, 8735−8739.
4. Jucker, F. M., Heus, H. A., Yip, P. F., Moors, E. H. M., and Pardi, A. (1996) *J. Mol. Biol. 264*, 968−980.
5. Glück, A., Endo, Y., and Wool, I. G. (1992) *J. Mol. Biol. 226*, 411−424.
6. Szewczak, A. A., Moore, P. B., Chan, Y.-L., and Wool, I. G. (1993) *Proc. Natl. Acad. Sci. U.S.A. 90*, 9581−9585.
7. Endo, Y., Glück, A., and Wool, I. G. (1991) *J. Mol. Biol. 221*, 193−207.
8. Orita, M., Nishikawa, F., Shimayama, T., Taira, K., Endo, Y., and Nishikawa, S. (1993) *Nucleic Acids Res. 21*, 5670−5678.
9. Orita, M., Nishikawa, F., Kohno, T., Senda, T., Mitsui, Y., Endo, Y., Taira, K., and Nishikawa, S. (1996) *Nucleic Acids Res. 24*, 611−618.
10. Endo, Y., Chan, Y.-L., Lin, A., Tsurugi, K., and Wool, I. G. (1988) *J. Biol. Chem. 263*, 7917−7920.
11. Chen, X.-Y., Link, T. M., and Schramm, V. L. (1998) *Biochemistry 37*, 11605−11613.
12. Engert, A., Sausville, E. A., and Vitetta, E. (1998) *Curr. Top. Microbiol. Immunol. 234*, 13−33.
13. O'Toole, J. E., Esseltine, D., Lynch, T. J., Lambert, J. M., and Grossbard, M. L. (1998) *Curr. Top. Microbiol. Immunol. 234*, 35−56.
14. Baluna, R., Rizo, J., Gordon, B. E., Ghetie, V., and Vitetta, E. S. (1999) *Proc. Natl. Acad. Sci. U.S.A. 96*, 3957−3962.
15. Chen, X.-Y., Berti, P. J., and Schramm, V. L. (2000) *J. Am. Chem. Soc. 122*, 1609−1617.
16. Chen, X.-Y., Berti, P. J., and Schramm, V. L. (2000) *J. Am. Chem. Soc. 122*, 6527−6534.
17. Horenstein, B. A., Parkin, D. W., Estupiñán, B., and Schramm, V. L. (1991) *Biochemistry 30*, 10788−10795.
18. Horenstein, B. A., and Schramm, V. L. (1993) *Biochemistry 32*, 7089−7097.
19. Chen, X.-Y., Link, T. M., and Schramm, V. L. (1996) *J. Am. Chem. Soc. 118*, 3067−3068.

20. Werner, R. M., and Stivers, J. T. (2000) *Biochemistry 39*, 14054−14064.
21. Damha, M. J., and Ogilvie, K. K. (1993) in *Methods in Molecular Biology: Protocols for Oligonucleotide and Analogues* (Agrawal, S., Ed.) pp 81−114, Humana Press, Totowa, NJ.
22. Evans, G. B., Furneaux, R. H., Gainsford, G. J., Schramm, V. L., and Tyler, P. C. (2000) *Tetrahedron 56*, 3053−3062.
23. Makino, K., and Ichikawa, Y. (1998) *Tetrahedron Lett. 39*, 8245−8248.
24. Hollis, T., Ichikawa, Y., and Ellenberger, T. (2000) *EMBO J. 19*, 758−766.
25. Usman, N., Ogilvie, K. K., Jiang, M.-Y., and Cedergren, R. J. (1987) *J. Am. Chem. Soc. 109*, 7845−7854.
26. Wu, T., Ogilvie, K. K., and Pon, R. T. (1989) *Nucleic Acids Res. 17*, 3501−3517.
27. Westman, E., and Strömberg, R. (1994) *Nucleic Acids Res. 22*, 2430−2431.
28. Gopaul, D. N., Meyer, S. L., Degano, M., Sacchettini, J. C., and Schramm, V. L. (1996) *Biochemistry 35*, 5963−5970.
29. Mazzella, L. J., Parkin, D. W., Tyler, P. C., Furneaux, R. H., and Schramm, V. L. (1996) *J. Am. Chem. Soc. 118*, 2111−2112.
30. Luyten, I., Thibaudeau, C., and Chattopadhyaya, J. (1997) *Tetrahedron 53*, 6903−6906.
31. Miles, R. W., Tyler, P. C., Evans, G. B., Furneaux, R. H., Parkin, D. W., and Schramm, V. L. (1999) *Biochemistry 38*, 13147−13154.
32. Schärer, O. D., Ortholand, J.-Y., Ganesan, A., Ezaz-Nikpay, K., and Verdine, G. L. (1995) *J. Am. Chem. Soc. 117*, 6623−6624.
33. Jespersen, T. M., Dong, W., Sierks, M. R., Skrydstrup, T., Lundt, I., and Bols, M. (1994) *Angew. Chem., Int. Ed. Engl. 33*, 1778−1779.
34. Ichikawa, M., Igarashi, Y., and Ichikawa, Y. (1995) *Tetrahedron Lett. 36*, 1767−1770.
35. Ichikawa, Y., and Igarashi, Y. (1995) *Tetrahedron Lett. 36*, 4585−4586.
36. Igarashi, Y., Ichikawa, M., and Ichikawa, Y. (1996) *Tetrahedron Lett. 37*, 2707−2708.
37. Bols, M. (1998) *Acc. Chem. Res. 31*, 1−8.
38. Ichikawa, Y., Igarashi, Y., Ichikawa, M., and Suhara, Y. (1998) *J. Am. Chem. Soc. 120*, 3007−3018.
39. Bülow, A., Plesner, I. W., and Bols, M. (2000) *J. Am. Chem. Soc. 122*, 8567−8568.
40. Watanabe, K., Honjo, E., Tsukamoto, T., and Funatsu, G. (1992) *FEBS Lett. 304*, 249−251.
41. Pallanca, A., Mazzaracchio, R., Brigotti, M., Carnicelli, D., Alvergna, P., Sperti, S., and Montanaro, L. (1998) *Biochim. Biophys. Acta*, 277−284.
42. Weston, S. A., Tucker, A. D., Thatcher, D. R., Derbyshire, D. J., and Pauptit, R. A. (1994) *J. Mol. Biol. 244*, 410−422.
43. Monzingo, A. F., and Robertus, J. D. (1992) *J. Mol. Biol. 227*, 1136−1145.
44. Yan, X., Hollis, T., Svinth, M., Day, P., Monzingo, A. F., Milne, G. W. A., and Robertus, J. D. (1997) *J. Mol. Biol. 266*, 1043−1049.
45. Kati, W. M., Acheson, S. A., and Wolfenden, R. (1992) *Biochemistry 31*, 7356−7366.
46. Wolfenden, R. (1999) *Bioorg. Med. Chem. 7*, 647−652.

BI010499P